Three-State Light Switch of $[Ru(phen)_2dppz]^{2+}$: Distinct Excited-State Species with Two, One, or No Hydrogen Bonds from Solvent

Johan Olofsson, Björn Önfelt,‡ and Per Lincoln*,†

Department Chemistry and Bioscience, Physical Chemistry, Chalmers University of Technology, S-412 96 Gothenburg, Sweden, and Department of Biological Sciences, Sir Alexander Fleming Building, Imperial College of Science, Technology and Medicine, London SW7 2AZ, United Kingdom

Received: December 22, 2003; In Final Form: March 19, 2004

The ruthenium complexes of dppz (dipyrido[3,2-*a*:2′,3′-*c*]phenazine) have found wide interest due to their environment-sensitive luminescence and are used, for example, as spectroscopic probes for DNA. The deactivation process for the excited state of the "light-switch" complex $[Ru(phen)_2dppz]^{2+}$ (phen = 1,10-phenanthroline) has been studied in water, glycerol, ethylene glycol, and 1,2- and 1,3-propandiol by using fluorescence spectroscopy and single photon counting. In all solvents anomalous temperature dependence is found (increasing quantum yield and excited-state lifetime with increasing temperature). Model-independent analysis shows that only two emissive species, with solvent- and temperature-invariant emission spectral profiles, are sufficient to account for all the data in the polyol solvents. Van't Hoff plots of the ratio of the two species are linear at higher temperatures in all solvents, indicating rapid thermal equilibration of the two species, except for lower temperatures in the most viscous solvent glycerol. Kinetic modeling of the system with microscopic rate constants with positive Arrhenius activation energies requires a third nonemissive species, which is assigned to an excited state with two hydrogen bonds from the solvent, whereas the first two species are assigned to the mono-hydrogen-bonded and non-hydrogen-bonded excited-state species. This assignment is supported by the observation of a growing luminescence intensity as temperature is increased, but no wavelength shift, of high-purity $[Ru(phen)_2dppz]^{2+}$ in water solution.

Introduction

Ru(II) complexes have attained considerable interest for the development of DNA conformational probes as well as of anticancer drugs[1−17] (Chart 1). A particularly interesting group of complexes have dipyrido[3,2-*a*:2′,3′-*c*]phenazine (dppz) as the ligand to ruthenium.[18−22] They luminesce extremely weakly in water,[23−29] but in nonaqueous solvent and upon binding to DNA[12,19,23,30−32] the luminescence is enhanced by a factor of >1000 compared to water ("light-switch effect").[12,19]

The Ru-dppz complexes bind strongly to DNA, but the excited-state lifetime, and consequently the luminescence quantum yield, shows a remarkable sensitivity to the chirality of the ruthenium center, the nature of the ancillary ligands, and the nucleic acid sequence.[33] To explain the structural sensitivity of the light-switch effect, it is of importance to fully understand the quenching mechanism of Ru-dppz complexes in an aqueous environment. The basic photophysical properties of Ru(II)-polypyridyl complexes are relatively well understood, and can be described by the charge-transfer model: when photoexcited with visible light, an electron in a d-orbital of ruthenium is transferred to an antibonding π^* orbital of one of the ligands, and after rapid intersystem crossing, a charge-separated state of triplet character with a lifetime on the order of microseconds is formed (metal-to-ligand charge-transfer, MLCT).[20,21,34−41] When L = 2,2′-bipyridine (bpy) or 1,10-phenanthroline (phen) in $[Ru(L)_2dppz]^{2+}$ the dppz ligand has the lowest lying π^* orbital, and there is a rapid localization of the charge transfer electron to dppz creating an excited state that formally can be described as a complex of the dppz anion radical with Ru(III)-$(L)_2$. There is considerable evidence for the efficient quenching of Ru-dppz complexes in water to be due to fast hydrogen bonding of solvent to the relatively basic phenazine aza nitrogens of the dppz anion radical.[18,24,28,29,32,42] A very short-lived intermediate MLCT state has indeed been detected in water, and suggested to be similar to the not hydrogen bonded dppz-localized state, which dominates the emission in DNA and in acetonitrile,[30] a conclusion that is supported also by time-resolved resonance Raman studies (TR^3).[23,33] However, the question whether just one or both of the aza nitrogens have to be hydrogen bonded to quench the emission has remained unanswered, although the answer is significant for the interpretation of the DNA luminescence data in structural terms.

Recently, increasing quantum yield with increasing temperature has been reported for $[Ru(bpy)_2dppz]^{2+}$ at low temperature in nitrile solvents.[4] The effect was attributed to an enthalpy-favored dark state, in which a more dppz-delocalized charge

CHART 1

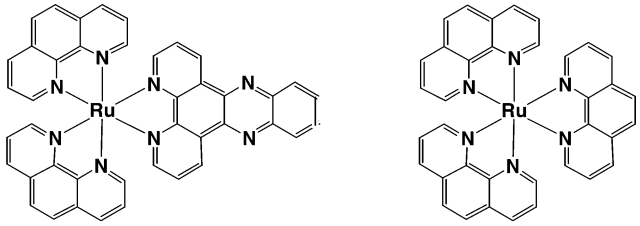

a. $[Ru(phen)_2dppz]^{2+}$ b. $[Ru(phen)_3]^{2+}$

* To whom correspondence should be addressed. Phone: +46 31 772 30 55. Fax: +46 31 772 38 58. E-mail: lincoln@chembio.chalmers.se.
‡ Chalmers University of Technology.
† Imperial College of Science, Technology and Medicine.

10.1021/jp037967k CCC: $27.50
Published on Web 04/28/2004

distribution is stabilized by interactions with the moderately polar solvent. Alternatively, a quantum-chemical study of the photophysics of Ru(II) complexes suggested the dark state to be the lowest dppz-ligand centered π^* triplet, and the increase in quantum yield with temperature due to the thermal population of an emitting ^{3}MLCT state that was predicted to be slightly higher in energy.[44] We have recently described a qualitatively similar behavior of $[Ru(phen)_2dppz]^{2+}$ in glycerol, but at considerably higher temperatures.[45] In this solvent, the unusual temperature behavior of the quantum yield and the excited-state lifetimes could be modeled by a simple kinetic model comprising two luminescent excited-state species that interconvert with microscopic rate constants having positive activation energies. On the basis of the enthalpy difference estimated from the activation energies, we assigned these two luminescent excited species in glycerol solution to be either non- or bis-hydrogen bonded to solvent.

In the present work we extend the study of the temperature dependence of the emission of $[Ru(phen)_2dppz]^{2+}$ to include also other hydroxylic solvents: ethylene glycol, 1,2- and 1,3-propandiol, ethanol, and water. Only two types of elementary emission spectral profiles were needed to fit all measured emission spectra in the three diols and glycerol in a large temperature range (10−150 °C) and the emission spectra of the two differently solvated species and their concentration profiles could be deconvoluted from the data. However, although the simple kinetic model, comprising two luminescent excited-state species and all-positive activation energies for the microscopic rate constants,[45] could excellently fit the temperature dependence of the total quantum yield, it failed to fit the concentration profiles. To retain all-positive activation energies for the microscopic rate constants, we had to include in the model a third, nonemissive, excited state. We assign this nonemissive state to be bis-hydrogen bonded, and the two emissive states to be mono- and non-hydrogen bonded. Support for this notion comes from the observation that the extremely low quantum yield of high-purity $[Ru(phen)_2dppz]^{2+}$ in water increases with temperature without appreciable change of the emission profile, consistent with the presence in aqueous solution of mainly bis- and some mono-hydrogen-bonded excited-state species.

Materials and Methods

Fluorescence Measurements. Steady-state emission measurements were carried out with Spex fluorolog-3 with the Datamax software. The concentration of $[Ru(phen)_2dppz]^{2+}$ was ca. 100 μM at all measurements. The wavelength of excitation was 440 nm and the steady-state emission intensity was measured in the range 450−1000 nm. The luminescence measurements were performed in a temperature range of −195 to 200 °C. Three devices were used to cover the temperature range: low-temperature measurements (−195 to 20 °C) were done in a nitrogen-cooled cryostat (Oxford instruments) with a temperature regulator, a circulating water bath (10−70 °C), and a cuvette holder built in-house with a heater (20−200 °C). The measurements above 150 °C are not included in the study because at higher temperatures irreversible spectral effects began to appear.

Time-Correlated Single-Photon Counting (TC-SPC). Laser pulses (≫20 ps duration) were generated from a tunable (700−1000 nm) Ti:Saphire oscillator (Tsunami, Spectra Physics 3960) operating at 880 nm with a frequency of 80 MHz. The pulses were passed through a pulse-picker (Spectra Physics 3980) changing the frequency of the pulse train to 4 MHz. The pulses were frequency doubled to 440 nm and passed through a wavelength selector, excluding residual IR, and finally through a (vertical) polarizer to ensure well-defined polarization of light used for excitation. Emission was collected at 90° in the horizontal plane relative to the propagation of the excitation beam through a polarizer set at the magic angle from the vertical polarization of the excitation beam. The detection unit was from Edingburough Instruments (OB-900 L) and contained a cell holder thermostated by a water jacket, a monochromator (≫16 nm bandwidth), and a water-cooled photomultiplier from Hamamatsu (C4878). The instrumental response function was recorded with use of a dilute sample of a scattering (latex) solution. The recorded fwhm for the response function was ≫140 ps when the Ti:Saphire laser was used and 1 ns when the diode was used.

SCHEME 1: Kinetic Model Scheme

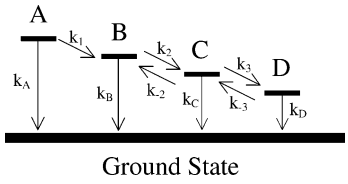

Singular-Value Decomposition. The steady-state emission spectra, recorded in various solvents at different temperatures, were collected as columns into a matrix **M**. By using the MatLab computational software, **M** was then factorized into three matrixes:

$$\mathbf{M} = \mathbf{U} \times \mathbf{S} \times \mathbf{V}^{\mathrm{T}} \tag{1}$$

where **S** is diagonal and **U** and **V** are orthonormal. The global **M** matrix with the dimension 191 × 72 was formed from the dataset of $[Ru(phen)_2dppz]^{2+}$ in glycerol, ethylene glycol, and 1,2- and 1,3- propandiol at 10−150 °C. The **U** matrix (191 × 72) is wavelength dependent with the most significant component in the first column. The diagonal of the **S** matrix (72 × 72) gives the weight of each component, the nonnegative singular values $\sigma_1 \geq \sigma_2 \geq ... \geq 0$. The columns of the **V** matrix (72 × 72) give information about how the components vary with temperature.

Kinetic Analysis. TCSPC traces were fitted to a sum of exponentials $[S(t) = \sum\alpha_i \exp(-t/\tau)]$, τ being the lifetime, with a deconvolution approach by using a homemade routine in the framework of the software package Matlab, allowing global analysis of several traces.

Kinetic Modeling. For a system of first-order reactions, the relation between the concentrations of the reacting species, expressed as a column vector of concentration values at a certain time $\mathbf{q}_t$, and the time derivatives of the concentrations is linear:

$$\frac{\mathrm{d}\mathbf{q}}{\mathrm{d}t} = \mathbf{L}\mathbf{q} \tag{2}$$

where **L** is a quadratic matrix containing the microscopic rate constants describing the processes. Neglecting the contribution from the relatively short-lived state A, for the three remaining excited states of Scheme 1 we get:

$$\mathbf{L} = \begin{bmatrix} -(k_B + k_2) & k_{-2} & 0 \\ k_2 & -(k_C + k_{-2} + k_3) & k_{-3} \\ 0 & k_3 & -(k_D + k_{-3}) \end{bmatrix} \quad \text{and}$$

$$\mathbf{q}_t = \begin{bmatrix} [B]_t \\ [C]_t \\ [D]_t \end{bmatrix} \tag{3}$$

Since species D is supposed to be nonemissive, a simpler two-

state model will be used when appropriate:

$$\mathbf{L}' = \begin{bmatrix} -(k_B + k_2) & k_{-2} \\ k_2 & -(k_C' + k_{-2}) \end{bmatrix} \text{ and } \mathbf{q}_t' = \begin{bmatrix} [B]_t \\ [C]_t \end{bmatrix} \quad (4)$$

Integration from time zero (excitation moment) gives an expression for the concentrations at time *t*:

$$\mathbf{q}_t = \mathbf{W}\,\mathrm{diag}(\mathbf{W}^{-1}\mathbf{q}_0)\begin{bmatrix} e^{\lambda_1 t} \\ e^{\lambda_2 t} \\ \dots \end{bmatrix} \qquad \mathbf{q}_0 = \begin{bmatrix} 1 \\ 0 \\ 0 \end{bmatrix} \quad (5)$$

where diag(**a**) denotes a diagonal matrix (the elements of vector **a** along the main diagonal and zero elsewhere), **W** is the eigenvector matrix that diagonalizes **L**, and the λ_i are the corresponding eigenvalues:

$$\mathbf{W}^{-1}\mathbf{L}\mathbf{W} = \mathrm{diag}\left(\begin{bmatrix} \lambda_1 \\ \lambda_2 \\ \dots \end{bmatrix}\right) \quad (6)$$

with the lifetimes $\tau_i = \lambda_i^{-1}$. In those cases in which the SPC decays could be analyzed satisfactorily with a single exponential (the diol solvents), only the longest calculated lifetime was included in the fitting, and for fitting the glycerol data the two longer calculated lifetimes were used. Under continuous illumination, the relative steady-state concentrations of the excited-state species are given by multiplication of the initial concentration vector with the inverse of the microscopic rate-constant matrix:

$$\mathbf{q}_{ss} = \mathbf{L}^{-1}\mathbf{q}_0 \quad (7)$$

Evaluating the inverse with Cramers rule gives the following expressions for the steady-state concentrations:

$$[B]_{SS} = \frac{1}{k_B + [k_2 k_C'/(k_{-2} + k_C')]} \quad (8)$$

and

$$\frac{[B]_{ss}}{[C]_{ss}} = \frac{k_{-2} + k_C'}{k_2} \quad (9)$$

where

$$k_C' = k_C + k_3 k_D (k_{-3} + k_D)^{-1} \quad (10)$$

Rate constants are supposed to follow an Arrhenius expression [$k_i = A \exp(-E_i/RT)$].

Chemicals. $[Ru(phen)_2dppz]Cl_2$ was synthesized as described elsewhere,[17] with the exception that the BF_4^- counterion was used for isolation and chromatography rather than the PF_6^-, a procedure that virtually eliminated the last traces of impurities (presumably $[Ru(phen)_3]^{2+}$) luminescent in water solution. Glycerol (>99.5%, spectrophotometric grade, water content less than 0.1%), ethylene glycol (>99.8%), 1,2-propandiol (>99.5%), and 1,3-propandiol (>99%) were purchased from Sigma-Aldrich. Argon purging of the glycerol solution did not change the emission intensity for either $[Ru(phen)_3]^{2+}$ or $[Ru(phen)_2dppz]^{2+}$ in the temperature range 10−150 °C.

Results

Figure 1 shows how the quantum yield (integrated steady-state emission intensity in the range 550−800 nm) for $[Ru(phen)_2dppz]^{2+}$ varies with temperature in the different solvents. The behavior is qualitatively similar in all solvents and goes through four phases as the temperature is increased: (a) the quantum yield is essentially solvent independent below the glass-forming temperature, (b) the quantum yield decreases as the solvent becomes less viscous to reach a minimum in the range from −50 to 60 °C, (c) upon further increasing temperature, the emission intensity increases to a local maximum occurring in the range 0−120 °C, and (d) the quantum yield again decreases with temperature and the curves of the different solvents appear to coincide in the high-temperature limit, interestingly, with a slope very similar to the corresponding curve of $[Ru(phen)_3]^{2+}$ in glycerol. The position and magnitude of the local maximum in phase c is sensitively dependent on solvent, for example, compare the results in 1,2- and 1,3- propanediol which only differ by the position of one hydroxyl group.

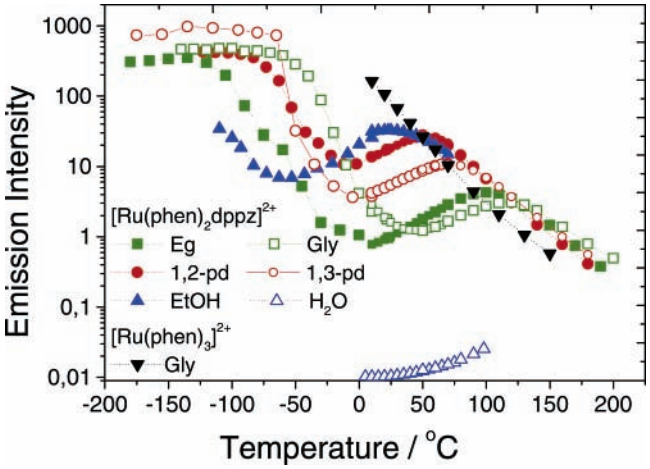

Figure 1. Integrated steady-state emission intensity (500−800 nm) as a function of temperature in different solvents. The wavelength of excitation is 440 nm. Key: $[Ru(phen)_2dppz]^{2+}$ in glycerol [Gly] (green open squares), ethylene glycol [Eg] (green solid squares), 1,2-propandiol [1,2-Pd] (red solid circle), 1,3-propandiol [1,3-Pd] (red open circle), ethanol [EtOH] (blue solid triangle), and water [H_2O] (blue open triangle) and $[Ru(phen)_3]^{2+}$ in glycerol [Gly] (black solid downward triangle).

The lifetimes of $[Ru(phen)_2dppz]^{2+}$ in glycerol, ethylene glycol, and 1,2- and 1,3-propandiol were determined by global fitting of traces measured with time-correlated single-photon counting (TC−SPC), and are plotted against temperature in Figure 2. Only for glycerol did a second, short lifetime contribute significantly (fractional intensity >1%) to the steady-state intensity.[45] The long lifetime followed the same behavior as the integrated luminescence intensity and ranged from 5.8 (ethylene glycol, 10 °C) to 104 ns (1,2-propandiol at 50 °C).

Also the shape and position of the emission band vary with solvent and temperature; Figure 3 shows some representative normalized spectra. Singular value decomposition (SVD, MatLab software) of the spectra obtained in this temperature range show that only two independent spectral species (components) are required to reproduce the data for each solvent (Table 1). For comparison, the SVD analysis of $[Ru(phen)_3]^{2+}$ in glycerol solution, the emission spectra of which were found to be essentially invariant with temperature, is also included. A global SVD analysis of the whole dataset of $[Ru(phen)_2dppz]^{2+}$ in the four polyol solvents (72 spectra) gave a third singular value slightly larger than the second (insignificant) value for $[Ru(phen)_3]^{2+}$. The three most significant wavelength-dependent **U** columns from the global SVD analysis, multiplied by their respective singular values, are shown in Figure 4, which clearly shows that only the two columns associated with the two largest singular values σ_1 and σ_2 are significant. The temperature

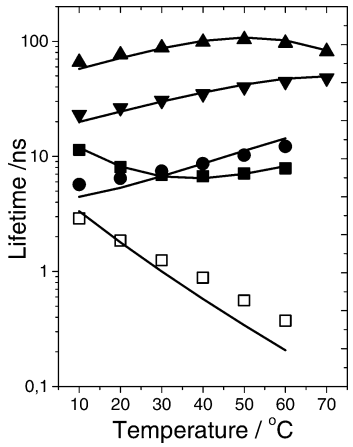

Figure 2. Lifetimes for the $[Ru(phen)_2dppz]^{2+}$ complex in glycerol (■, □), ethylene glycol (●), 1,2-propandiol (▲), and 1,3-propandiol (▼) are shown. The lines represent the best fit of the kinetic model to the data. The lifetimes were determined by global fitting (MATLAB software) of traces from time-correlated single-photon counting (tc-SPC).

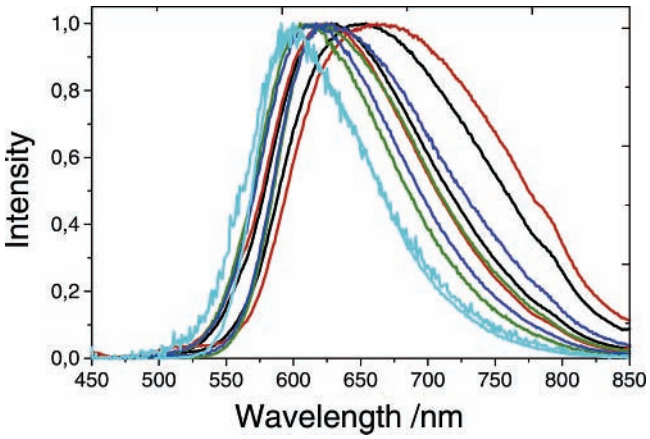

Figure 3. Most blue- and red-shifted steady-state emission spectra for $[Ru(phen)_2dppz]^{2+}$ in glycerol [black line] (the temperature for the most red-shifted spectrum to the right) at 140 and 60 °C, ethylene glycol [red line] at 150 and 10 °C, 1,2-propandiol [green line] at 150 and 10 °C, and 1,3-propandiol [dark blue line] at 140 and 10 °C. Also shown are the two most extreme spectra of $[Ru(phen)_3]^{2+}$ in glycerol [light blue line], which almost coincide (10 and 140 °C). All spectra are normalized to unit maximum intensity to emphasize the spectral profile shift with temperature.

TABLE 1: Singular Values from SVD-analysis of the Steady-State Emission Spectra for the Metal Complexes in Different Solvents[a]

	σ_1	σ_2	σ_3
$[Ru(phen)_3]^{2+}$ in glycerol	100	0.51	0.3538
$[Ru(phen)_2dppz]^{2+}$ in glycerol	100	7.2405	0.6017
$[Ru(phen)_2dppz]^{2+}$ in ethylene glycol	100	8.0719	0.2139
$[Ru(phen)_2dppz]^{2+}$ in 1,2-propandiol	100	3.6947	0.1159
$[Ru(phen)_2dppz]^{2+}$ in 1,3-propandiol	100	5.1489	0.1959
$[Ru(phen)_2dppz]^{2+}$ in all 4 solvents	100	11.0375	1.2551

[a] The largest singular value (σ_1) is normalized to 100.

dependence of the two most significant columns of the **V** matrix are shown in Figure 5a−d. (the third **V** column is not shown as it displays a very irregular temperature dependence). Thus, the columns $\mathbf{u}_1$, $\mathbf{u}_2$, $\mathbf{v}_1$, and $\mathbf{v}_2$ of the **U** and **V** matrixes account for the matrix $\mathbf{I}_{SS}$ containing all 72 experimental spectra:

$$\mathbf{I}_{SS} = \mathbf{USV}^T = [\sigma_1\mathbf{u}_1\sigma_2\mathbf{u}_2][\mathbf{v}_1\mathbf{v}_2]^T = [\mathbf{b}_{(wl)}\mathbf{c}_{(wl)}][\mathbf{b}_T\mathbf{c}_T]^T \quad (11)$$

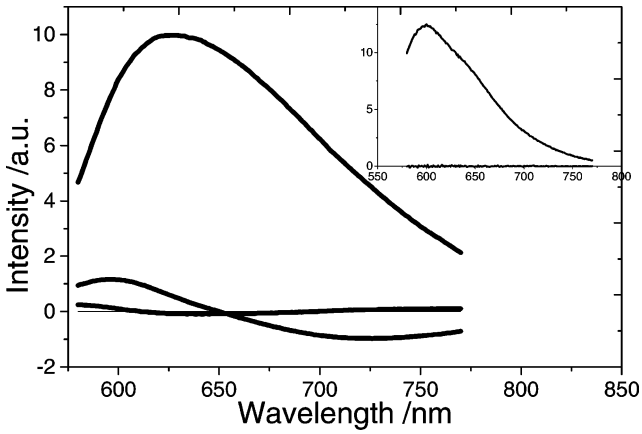

Figure 4. Principal components from a global SVD analysis of $[Ru(phen)_2dppz]^{2+}$ in glycerol, ethylene glycol, and 1,2- and 1,3-propandiol. The **U**-vectors of the three largest principal components multiplied by their respective singular values are shown. The inset also shows the products of the **U**-vector multiplied by their singular values for $[Ru(phen)_3]^{2+}$ in glycerol.

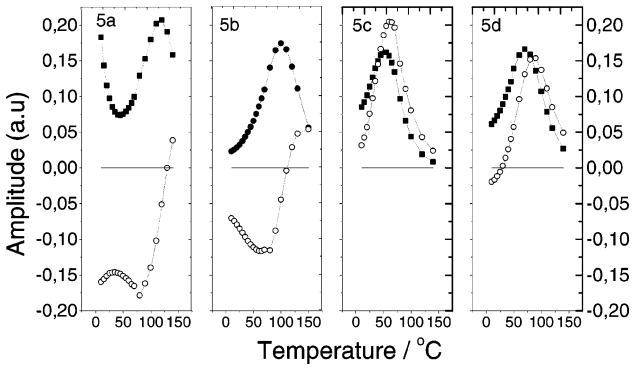

Figure 5. **V** vectors from the SVD analysis of the steady-state emission intensity showing the temperature evolution of the two principal components of interest for the $[Ru(phen)_2dppz]^{2+}$ in different solvents. The global SVD analysis was performed in the following four solvents: glycerol [a], ethylene glycol [b], and 1,2- [c] and 1,3-propanediol [d]. The first [■] (singular value =100) and second [○] (singular value = 11) components are shown.

It should be noted that the SVD components have no physical correspondence, but they demonstrate that only two emissive species, **b** and **c**, are involved. Species **b** and **c** are connected to the SVD components through a transformation matrix **R**, the rows of which are uniquely determined simply by the criteria of nonnegativeness for the emission and concentration profiles:

$$[\sigma_1\mathbf{u}_1\sigma_2\mathbf{u}_2]\mathbf{R}^{-1} = [\mathbf{b}_{(wl)}\mathbf{c}_{(wl)}] \geq 0 \quad (12)$$

$$[\mathbf{v}_1\mathbf{v}_2]\mathbf{R}^T = [\mathbf{b}_{(T)}\mathbf{c}_{(T)}] \geq 0 \quad (13)$$

with $\mathbf{b}_{(wl)}$ being the emission profile for species B_x and $\mathbf{b}_{(T)} = [B]_{SS}$, the steady-state concentration of B as a function of the temperature T, and correspondingly for species C.

Figure 6 shows the emission profiles obtained accordingly and Figure 7 the corresponding concentration profiles. Although the species profiles are well defined, the relative scaling between the two species is still arbitrary. It was settled by the ratio of the corresponding α-values from the time-correlated SPC data for glycerol and ethylene glycol[45] (data not shown).

Despite the fact that the calculated concentrations show a non-Arrhenius behavior, a plot of the logarithm of the *ratio* between the calculated concentration profiles, ln([B]/[C]), against the inverse of the temperature, $1/T$, gives a single straight

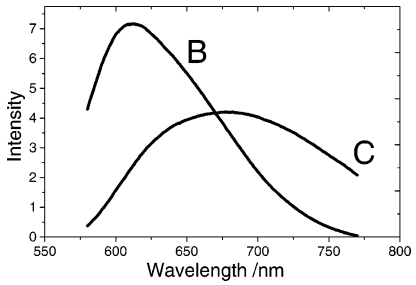

Figure 6. Temperature-independent emission spectra of the "B" and "C" species calculated according to eq 12.

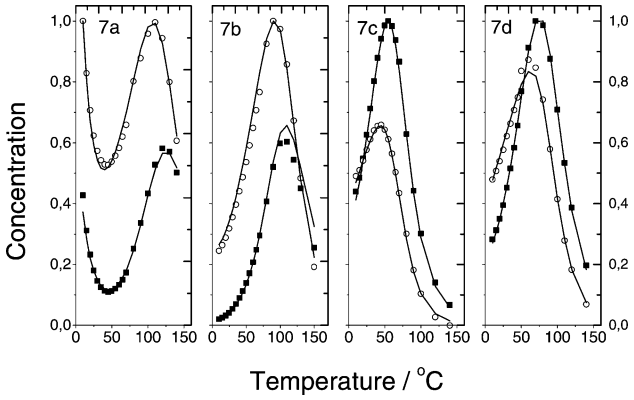

Figure 7. Concentrations of the B [■] and C [○] species of $[Ru(phen)_2dppz]^{2+}$ in glycerol [a], ethylene glycol [b], and 1,2- [c] and 1,3-propanediol [d] calculated according to eq 13. The line represents the best fit of the kinetic model to the data.

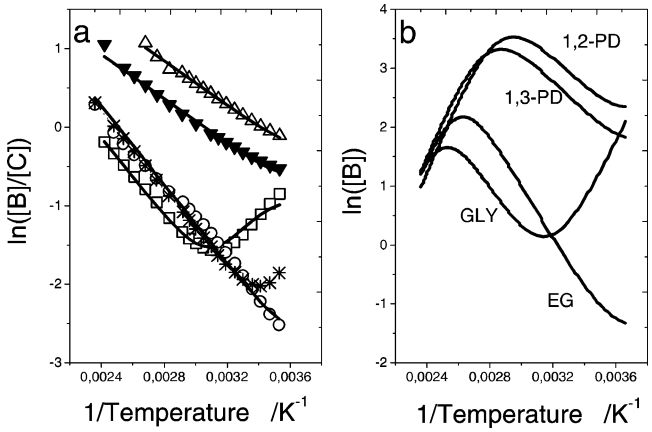

Figure 8. (a) Van't Hoff plot of the ratio between the steady-state concentrations of the B and C species for the solvents glycerol (□), ethylene glycol (○), and 1,2- (△) and 1,3-propandiol (▼). The line represents the best fit to the explicit three-state kinetic model for ethylene glycol and glycerol, and to the two-state kinetic model for the propandiols; the best fit of the two-state kinetic model to the ethylene glycol data is denoted by the curve with asterisks. (b) Van't Hoff plot of the steady-state concentration of species B.

line for ethylene glycol and 1,2- and 1,3-propandiol and two linear regions for glycerol (Figure 8a). This is a key observation that strongly supports the notion of a rapid equilibrium between B and C in the high-temperature linear regions, i.e., that $[B]_{SS} = K_{BC}[C]_{SS}$ where

$$\ln K_{BC} = -\frac{\Delta H^\circ_{BC}}{RT} + \frac{\Delta S^\circ_{BC}}{R} \qquad (14)$$

with the enthalpy (ΔH°_{BC}) and the entropy (ΔS°_{BC}) terms being independent of temperature. Comparison with the steady-state expression, eq 9, suggests that $k_{-2} \gg k_C'$ and thus that $K_{BC} = k_{-2}/k_2$ with both k_{-2} and k_2 being elementary rate constants obeying the Arrhenius equation with positive activation energies. The negative slope found for the diols in the plot ln([B]/[C]) vs $1/T$ is thus $[E_a(k_2) - E_a(k_{-2}))]/R$, showing that the reverse reaction step k_{-2} has the larger activation energy and, thus, the stronger dependence on temperature. If $k_{-2} \gg k_C'$, as suggested above, the steady-state expression for [B] simplifies to:

$$[B]_{SS} = \frac{1}{k_B + (k_2 k_C'/k_{-2})} \qquad (15)$$

The plot of ln[B] against $1/T$ shows two linear regions for the diol solvents. In the high-temperature region, k_{-2} is large also compared to k_2 and B is the only species present, with $[B] = (k_B)^{-1}$. Interestingly, the value of the activation energy of k_B is virtually the same in all solvents, and is almost identical with that of the decay of tris(1,10-phenanthroline)ruthenium(II) in glycerol.

In the low-temperature linear region of the diol solvents, $[B] = k_{-2}/k_2k_C'$ and the slope of ln([B]) vs $1/T$ is more negative than the corresponding slope of the ratio ln([B]/[C]), indicating that the activation energy of k_C' is negative. Although this conclusion is not consistent with k_C' describing a single, elementary reaction step, the result can readily be explained in a three-state model (Scheme 1), in which k_C' is composed of elementary rate constants according to eq 10: $k_C' = k_C + k_3k_D(k_{-3} + k_D)^{-1}$.

Kinetic Modeling and Fitting to Data. The full three-state model (eq 3) involves seven microscopic rate constants each obeying the Arrhenius expression $k_i = A_i \exp(-E_a(k_i)/RT)$, thus a total of 4×14 parameters for a fit to all four solvents. To reduce that large number, some simplifying assumptions were made. We assume for simplicity the rates of direct decay to the ground-state k_C to be identical to k_B, but the data could equally well be fitted with the restrictions $A(k_C) = A(k_B)$ and $E_a(k_C) = E_a(k_B) - 6$ kJ/mol (corresponding to k_C being an order of magnitude larger at 298 K, as predicted by the energy gap law[46]) with negligible changes in the values of the other parameters. We further assume that the activation energies for hydrogen bond formation or breaking at the two aza nitrogens are independent of whether the other nitrogen receives a hydrogen bond or not, i.e., we assume that $E_a(k_2) = E_a(k_3)$ and $E_a(k_{-2}) = E_a(k_{-3})$. The three-state model was strictly needed only for the fitting of the glycerol data (although it produced a better fit in the low-temperature range of the ethylene glycol data), and the two-state model (eq 4) with $k_C' = k_3k_D(k_{-3})^{-1}$ was used instead for the three diols. Further restrictions were imposed on the model by assuming that all activation energies E_a have the same values in the 1,2- as in the 1,3-propanediol solvent (two-state model), and in glycerol and ethylene glycol (three-state model), and that $E_a(k_B)$ is the same in all four solvents, the latter assumption supported by the convergence of slopes at high temperature in Figure 1. In all cases, the steady-state values $[B]_{SS}$ and $[B]_{SS}/[C]_{SS}$ and excited-state lifetimes as a function of temperature were calculated with eqs 7 and 6 and fitted to the ones determined experimentally with a least-squares error criterion. The fit of the kinetic models was quite good as judged by Figures 2, 7, 8, and 9.

Discussion

An interesting observation is that the quantum yield in the polyol solvents coincides at higher temperatures for $[Ru(phen)_2dppz]^{2+}$ and that the decrease in quantum yield with temperature there becomes similar to that for $[Ru(phen)_3]^{2+}$ in

SCHEME 2: Schematic Model of the Relaxation Pathways[a]

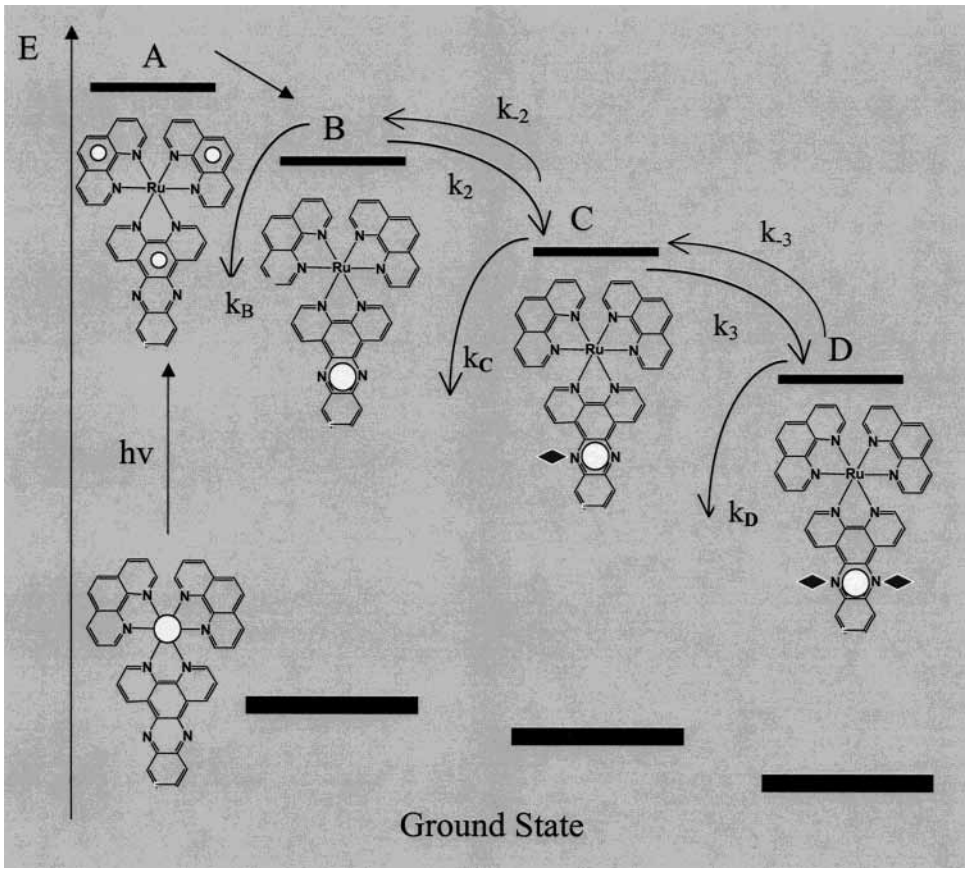

[a] Upon excitation of an electron from a d-orbital in ruthenium (ground state) the negative charge from the excited electron is distributed over the three ligands and forms a MLCT state (state A). The A state converts to another MLCT state B (no hydrogen bond) where the electron is localized on the dppz ligand. States C and D are two states which correspond to one or two solvent molecules hydrogen bonded to the phenazine nitrogens on the dppz ligand

glycerol. The solvent molecules cannot hydrogen bond to $[Ru(phen)_3]^{2+}$, in contrast to $[Ru(phen)_2dppz]^{2+}$, which results in a temperature-independent emission profile for the former because only one emissive state is populated. The SVD analysis of the emission spectra of $[Ru(phen)_2dppz]^{2+}$ shows that two independent fluorescent species are sufficient to describe the temperature dependence of the emission profile (Table 1) in the four polyol solvents.

We assume that the spectral profile for these species are temperature independent similarly to $[Ru(phen)_3]^{2+}$, which is supported by the finding that both the emission profiles and intensities converge at higher temperatures for $[Ru(phen)_2dppz]^{2+}$ in all four solvents. The latter observation suggests not only that species B has a temperature-independent spectral profile, but also that its spectral profile *and* its quantum yield (in the absence of hydrogen bonds from solvent) are independent of the nature of the polyol. Thus, it seems reasonable to assume, in these four rather similar solvents, the same solvent independence for the spectral profile and the quantum yield of the other species, C, as well.

The two significant components from the SVD analysis should thus correspond to two distinct emissive species, one solvated and one unsolvated form and a linear combination of the **V** and **U** vectors gives the concentration of the different species against temperature and the physical emission profiles, respectively. With the criteria that the concentration and the emission profiles should be nonnegative a unique linear combination was found (the **R** matrix in eqs 12 and 13). This analysis agrees qualitatively so far with our previous work in glycerol[45] where the two species corresponding to no and two hydrogen bonds was inferred. However, preliminary modeling of the experimental data showed that the two-state model was insufficient to describe the process with microscopic binding constants with positive activation energies. At lower temperatures in glycols, states B and C are in thermal equilibrium but the slope of ln([B]/[C]) against $1/T$ in (Figure 8a) is larger than ln([B]) against $1/T$ (Figure 8b), indicating that k_C' is negative. Thus the disappearance of C is not an elementary reaction (with microscopic rate constants having positive activation energies) and the simplest model that can explain this behavior is a model with a third nonemissive, "dark" state included. The existence of a third state that is nonemissive is in fact supported by observation that the emission profile in water does not change with temperature, although the intensity increases. This can be explained with water being a very effective hydrogen bond donor and only mono- and double-hydrogen-bonded excited-state molecules are present. The full three-state model involved 14 parameters (Schemes 1 and 2) from the beginning but the model can be simplified to 10 parameters and still describe the experimental data very well by using the following two assumptions: (a) The rate constants for deactivation from state B and C are equal, $k_B = k_C$ (Table 2) and (b) the activation energies for deactivation from the unsolvated B state are the same in all solvents studied. An observation that supports this is the convergence (a similar slope) of the quantum yield at higher temperatures. In 1,2- and 1,3-propandiols the data could be fit with identical sets of activation energies. The preexponential factor for formation of the first hydrogen-bonded species

TABLE 2: Activation Parameters for Microscopic Rate Constants of Excited-State Relaxation of $[Ru(phen)_2dppz]^{2+}$ in Glycerol, Ethylene Glycol, and 1,2- and 1,3-Propandiol[a]

process	GLY ln(*A*/s) [E_a (kJ mol^{-1})]	EG ln(*A*/s) [E_a (kJ mol^{-1})]	EG ln(*A*/s) [E_a (kJ mol^{-1})]	1,2-PD ln(*A*/s) [E_a (kJ mol^{-1})]	1,3-PD ln(*A*/s) [E_a (kJ mol^{-1})]
k_2	37.2 [41.9]	41.6 [41.9]	39.6 [41.9]	39.6 [45.6]	40.4 [45.6]
k_{-2}	43.2 [62.9]	47.9 [62.9]	45.8 [62.9]	44.4 [57.4]	44.7 [57.4]
k_3	36.3 [41.9]	38.8 [41.9]			
k_{-3}	48.8 [62.9]	51.9 [62.9]			
k_B	33.3 [53.2]	33.6 [53.2]	34.2 [53.2]	34.8 [53.2]	34.6 [53.2]
k_C	33.3 [53.2]	33.6 [53.2]			
k_D	24.6 [2.1]	24.6 [2.1]			
k_C'	12.1[b] [−19.0][b]	11.5[b] [−19.0][b]	11.8 [−17.7]	12.8 [−10.6]	13.6 [−10.6]

[a] Activation parameters were determined from fitting of concentrations and macroscopic rate constants shown in Figures 2 and 7. [b] ln(*A*) and E_A calculated with eq 10.

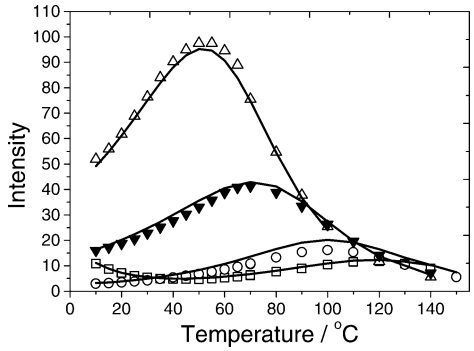

Figure 9. Quantum yield (integrated steady-state emission intensity) for $[Ru(phen)_2dppz]^{2+}$ in glycerol (□), ethylene glycol (○), and 1,2- (△) and 1,3-propandiol (▼). The solid line is the calculated best fit of the kinetic model to the data.

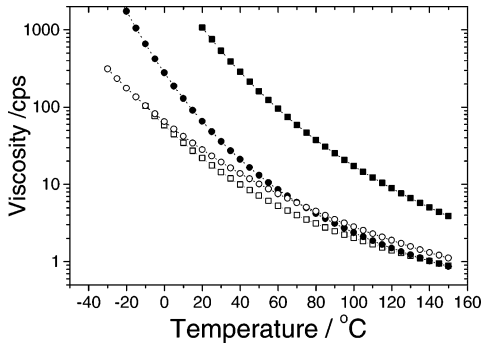

Figure 10. Temperature dependence of the viscosity in glycerol [■], ethylene glycol [□], and 1,2- [●] and 1,3-propanediol [○] (data from ref 48).

C with one hydrogen bond is two times larger for 1,3- than for 1,2-propanediol. We suggest that the secondary hydroxy groups do not easily form hydrogen bonds to the phenazine aza nitrogens because they are sterically hindered. From that it follows that the effective concentration of hydrogen binding hydroxy groups is two times larger for 1,3- than 1,2- propanediol, and the parameters from our model when fitting the experimental data give the ratio between rate constants of 2.2 (Table 2).

However, for EG and glycerol it is harder to compare the activation parameters in the full three-state model (eq 3) because more parameters are included and depend on each other. The much lower rates of especially k_{-2} in glycerol compared to ethylene glycol suggest that it depends strongly on viscosity (Table 2 and Figure 10). In all solvents there is a fast equilibrium between state B and state C (Scheme 2), except in glycerol at lower temperatures, and the enthalpy for breaking a hydrogen bond in the different solvents can easily be calculated from Figure 8a and the results are shown in Table 3. The enthalpy

TABLE 3: Enthalpy Change for Breaking a Hydrogen Bond to the Metal Complex Has Been Calculated from the Variation of the Ratio [B]/[C] with Temperature in Glycerol, Ethylene Glycol, and 1,2- and 1,3-Propandiol

$[Ru(phen)_2dppz]^{2+}$ in different solvents	ΔH (kJ mol^{-1})
glycerol	19
ethylene glycol	20
1,2-propandiol	11
1,3-propandiol	14

for breaking a hydrogen bond between two hydroxyl groups has been estimated to be ∼30 kJ mol^{-1}.[47] The calculated enthalpy values (Table 3) are significantly less compared to the literature values,[47] which is not unexpected since the values reflect a net difference in hydrogen bonding including solvent−solvent interactions. We note that the enthalpy difference (42 kJ/mol) between state B and state D calculated from the data of Table 2 is similar but slightly lower than the value estimated by the two-state model in our previous paper.[45]

Conclusion

Model-independent analysis of steady-state emission spectra obtained from $[Ru(phen)_2dppz]^{2+}$ in four polyol solvents at a range of temperatures show that only two emissive species, B and C, assumed to have solvent- and temperature-invariant emission spectral profiles, are sufficient to account for all the data. Van't Hoff plots of ln([B]/[C]) against T^{-1} are linear at higher temperatures in all solvents, indicating rapid thermal equilibration of the two species, except at the lower temperatures in the most viscous solvent glycerol. So far the simple two-state model of our previous report is consistent with the new data; however, the van't Hoff plots show the enthalpy difference between state B and C to be much smaller than previously estimated.[45] Thus, with B being the non-hydrogen-bonded excited-state species, C has to be reassigned to be the mono-hydrogen-bonded excited-state species, i.e., not being the bis-hydrogen-bonded species previously suggested. Furthermore, the kinetic modeling of the temperature dependence of the steady-state concentrations of B and C, with microscopic rate constants having positive Arrhenius activation energies, show that a third, nonemissive species D has to be included in the model. On the basis of estimated enthalpy differences, we assign this dark state to the excited state with two hydrogen bonds from the solvent. Support for this assignment comes from the observation of a growing luminescence intensity as temperature is increased, but no wavelength shift, of high-purity $[Ru(phen)_2dppz]^{2+}$ in water solution. Finally, it should be noted that, although the simplistic no, one, and two hydrogen bond assignment presented here provides an excellent quantitative explanation to the present data, a qualitatively very similar

temperature dependence of the luminescence intensity has been found in aprotic solvents,[43] and recent theoretical considerations point out the dppz-ligand centered triplet as a plausible candidate for an enthalpy-favored dark state in nonaqueous solvents.[44]

References and Notes

(1) Erkkila, K. E.; Odom, D. T.; Barton, J. K. *Chem. Rev.* **1999**, *99*, 2777.
(2) Nordèn, B.; Lincoln, P.; Åkerman, B.; Tuite, E. In *Metal Ions in Biological Systems*; Siegel, A., Siegel, H., Eds.; Marcel Dekker: New York, 1996; Vol. 33, p 177.
(3) Lincoln, B.; Broo, A.; Nordèn, B. *J. Am. Chem. Soc.* **1996**, *118*, 2644.
(4) Haq, I.; Lincoln, P.; Suh, D.; Nordèn, B.; Chowdhry, B. Z.; Chaires, J. B. *J. Am. Chem. Soc.* **1995**, *117*, 4788.
(5) Choi, S. D.; Kim, M. S.; Kim, S. K.; Lincoln, P.; Tuite, E.; Nordèn, B. *Biochemistry* **1997**, *36*, 214.
(6) Holmlin, R. E.; Stemp, E. D. A.; Barton, J. K. *Inorg. Chem.* **1998**, *37*, 29.
(7) Tuite, E.; Lincoln, P.; Nordèn, B. *J. Am. Chem. Soc.* **1997**, *119*, 239.
(8) Dupureur, C. M.; Barton, J. K. *J. Am. Chem. Soc.* **1994**, *116*, 10286.
(9) Dupureur, C. M.; Barton, J. K. *Inorg. Chem.* **1997**, *36*, 33.
(10) Hartshorn, R. M.; Barton, J. K. *J. Am. Chem. Soc.* **1992**, *114*, 5919.
(11) Jenkins, Y.; Friedman, A. E.; Turro, N. J.; Barton, J. K. *Biochemistry* **1992**, *31*, 10809.
(12) Friedman, A. E.; Kumar, C. V.; Turro, N. J.; Barton, J. K. *Nucleic Acids Res.* **1991**, *19*, 2595.
(13) Lincoln, B.; Norden, B. *Chem. Commun.* **1996**, *18*, 2145.
(14) Önfelt, B.; Lincoln, P.; Nordén, B. *J. Am. Chem. Soc.* **2001**, *123*, 3630.
(15) Önfelt, B.; Göstring, L.; Lincoln, P.; Nordén, B.; Önfelt, A. *Mutagenesis* **2002**, *17*, 317.
(16) Önfelt, B.; Lincoln, P.; Nordén, B. *J. Am. Chem. Soc.* **1999**, *121*, 10846.
(17) Hiort, C.; Lincoln, P.; Nordén, B. *J. Am. Chem. Soc.* **1993**, *115*, 3448.
(18) Chambron, J.-C.; Sauvage, J.-P.; Amouyal, E.; Koffi, P. *Nouv. J. Chim.* **1985**, *9*, 527.
(19) Friedman, A. E.; Chambron, J. C.; Sauvage, J. P.; Turro, N. J.; Barton, J. K. *J. Am. Chem. Soc.* **1990**, *112*, 4960.
(20) Krausz, E.; Ferguson, J. *Prog. Inorg. Chem.* **1989**, *37*, 293.
(21) Forster, L. S. *Coord. Chem. Rev.* **2002**, *227*, 59.
(22) Chen, P. Y.; Meyer, T. J. *Chem. Rev.* **1998**, *98*, 1439.
(23) Coates, C. G.; Olofsson, J.; Coletti, M.; McGarvey, J. J.; Önfelt, B.; Lincoln, P.; Nordèn, B.; Tuite, E.; Matousek, P.; Parker, A. W. *J. Phys. Chem. B* **2001**, *105*, 12653.
(24) Chambron, J.-C.; Sauvage, J.-P. *Chem. Phys. Lett.* **1991**, *182*, 603.
(25) Guo, X. Q.; Castellano, F. N.; Li, L.; Lakowicz, J. R. *Biophys. Chem.* **1998**, *71*, 51.
(26) Sabatani, E.; Nikol, H. D.; Gray, H. B.; Anson, F. C. *J. Am. Chem. Soc.* **1996**, *118*, 1158.
(27) Stoeffler, H. D.; Thornton, N. B.; Temkin, S. L.; Schanze, K. S. *J. Am. Chem. Soc.* **1995**, *117*, 7119.
(28) Yam, V. W. W.; Lo, K. K.-W.; Cheung, K. K.; Kong, R. Y. C. *Chem. Commun.* **1995**, *11*, 1191.
(29) Nair, R. B.; Cullum, B. M.; Murphy, C. J. *Inorg. Chem.* **1997**, *36*, 962.
(30) Olson, E. J. C.; Hu, D.; Hörmann, A.; Jonkman, A. M.; Arkin, M. R.; Stemp, E. D. A.; Barton, J. K.; Barbara, P. F. *J. Am. Chem. Soc.* **1997**, *119*, 11458.
(31) Önfelt, B.; Lincoln, P.; Nordén, B.; Baskin, J. S.; Zewail, A. H. *Proc. Natl. Acad. Sci. U.S.A.* **2000**, *97*, 5708.
(32) Amouyal, E.; Homsi, A.; Chambron, J.-C.; Sauvage, J.-P. *Dalton Trans.* **1990**, *6*, 1841.
(33) Olofsson, J.; Önfelt, B.; Lincoln, B.; Nordén, B.; Matousek, P.; Parker, A. W.; Tuite, E. *J. Inorg. Biochem.* **2002**, *91*, 286.
(34) Kober, E. M.; Sullivan, B. P.; Meyer, T. J. *Inorg. Chem.* **1984**, *23*, 2098.
(35) Kober, E. M.; Meyer, T. J. *Inorg. Chem.* **1982**, *21*, 3967.
(36) Karki, L.; Hupp, J. T. *Inorg. Chem.* **1997**, *36*, 3318.
(37) Bradley, P. G.; Kress, N.; Hornberger, B. A.; Dallinger, R. F.; Woodruff, W. H. *J. Am. Chem. Soc.* **1981**, *103*, 7441.
(38) Sykora, M.; Kincaid, J. R. *Inorg. Chem.* **1995**, *34*, 5852.
(39) Barigelletti, F.; Juris, A.; Balzani, V.; Belser, P.; Vonzelewsky, A. *J. Phys. Chem.* **1986**, *90*, 5190.
(40) Masschelein, A.; Jacquet, L.; Kirschdemesmaeker, A.; Nasielski. *J. Inorg. Chem.* **1990**, *29*, 855.
(41) Barigelletti, F.; Juris, A.; Balzani, V.; Belser, P.; Vonzelewsky, A. *Inorg. Chem.* **1983**, *22*, 3335.
(42) Schoonover, J. R.; Bates, W. D.; Meyer, T. J. *Inorg. Chem.* **1995**, *34*, 6421.
(43) Brennaman, M. K.; Alstrum-Acevedo, J. H.; Fleming, C. N.; Jang, P.; Meyer, T. J.; Papanikolas, J. M. *J. Am. Chem. Soc.* **2002**, *124*, 15094.
(44) Pourtois, G.; Beljonne, D.; Moucheron, C.; Schumm, S.; Kirsch-De Mesmaeker, A.; Lazzaroni, R.; Brédas, J.-L. *J. Am. Chem. Soc.* **2004**, *126*, 683.
(45) Önfelt, B.; Olofsson, J.; Lincoln, P.; Nordén, B. *J. Phys. Chem. A* **2003**, *107*, 1000.
(46) Caspar, J. V.; Meyer, T. J. *J. Am. Chem. Soc.* **1983**, *105*, 5583.
(47) Maskil, H. *The physical basis of organic chemistry*; Oxford University Press: New York, 1985.
(48) Yaws, C. L. *Handbook of Viscosity*; Gulf Publishing Co.: Houston, TX, 1995; Vol. 1.